

# AgentsCAD: Automated Design for Manufacturing of FDM Parts via Multi-Agent LLM Reasoning and Geometric Feature Recognition

Emmanuel George, Christopher Keefe, Peter Pak, and Amir Barati Farimani\*

*Department of Mechanical Engineering, Carnegie Mellon University, Pittsburgh, PA, USA*

E-mail: barati@cmu.edu

## Abstract

Parts manufactured with Fused Deposition Modeling (FDM) often require Design for Additive Manufacturing (DFAM) modifications to ensure printability, structural integrity, and reduced post-processing. Current slicers identify defects such as steep overhangs but are unable to modify the underlying geometry. This work presents *AgentsCAD*, a multi-agent system that bridges raw boundary-representation (B-Rep) geometry and Large Language Model (LLM) reasoning to automate targeted DFM. The workflow begins by parsing a STEP file. The agentic system detects overhangs above a 45° threshold, constructs a face-adjacency topology graph, and optionally injects semantic feature labels from a GraphSAGE model trained on MFCAD++ (59,665 parts), before dispatching a Claude Sonnet design-reasoning agent that recommends reorientations, fillets, chamfers, and similar modifications. A GPT-4o vision-language verifier inspects rendered views to confirm geometric integrity. Outputs include a modified STEP file and a human-readable report. A test case on a birdhouse model demonstrates that the

system correctly diagnoses overhangs, selects appropriate defect mitigation strategies, and proposes physically valid corrections, partially solving the geometry-to-language translation problem central to LLM-driven CAD modification.

# 1 Introduction

Fused Deposition Modeling (FDM) is an additive manufacturing process which builds parts layer by layer through depositing material along a sequence of two-dimensional cross-sections.<sup>1-3</sup> Since each new layer must rest upon the one beneath it, downward-facing surfaces tilted beyond roughly 45° from vertical (overhangs) are difficult to print reliably without supports or geometric modification. Design for Additive Manufacturing (DFAM)<sup>3,4</sup> addresses these limitations by reshaping geometry to improve dimensional accuracy, mechanical strength, and print efficiency while minimizing post-processing. Modern slicing software can flag problematic regions and generate support structures, but corrective decisions must be made by the engineer, who must iterate manually between CAD and slicer platforms until the part is suitable for printing.

A small but rapidly growing body of work has begun applying language and vision-language models at the CAD interface, organized in recent surveys along generation, modification, and analysis axes.<sup>5,6</sup> On the generation side, Text2CAD produces sequential CAD designs from natural-language prompts spanning beginner-to-expert detail,<sup>7</sup> Query2CAD generates parametric models directly from natural-language queries using FreeCAD,<sup>8</sup> and CADSmith<sup>9</sup> utilizes CADQuery based Python bindings to generate parametric models. ChatCAD extends this idea to multimodal LLM-guided CAD drawing restoration in zero-shot settings,<sup>10</sup> and CADCodeVerify uses vision-language models to validate generated CAD code.<sup>11</sup> In additive manufacturing specifically, large language models have been applied to the domain of defect prediction in various build monitoring tasks,<sup>2,3,12</sup> complementing real-time vision-based defect-detection systems for FFF printing.<sup>13</sup> These systems share a common pattern in that language or images map to new geometry or to defect classes, but no system to the authors' knowledge

modifies an existing part’s underlying B-Rep for more favorable manufacturing conditions.

Complementary literature on Automatic Feature Recognition (AFR) provides the geometric understanding needed to fill that gap.<sup>14</sup> Early work used hand-engineered rules and shallow neural networks to map manufacturing features from CAD geometry.<sup>15,16</sup> The deep-learning era brought volumetric approaches: 3D ShapeNets pioneered learned representations of 3D shape from voxel grids,<sup>17</sup> and subsequent 3D CNNs added gradient-based visual explanations for machining feature recognition.<sup>18</sup> More recent work returns to the native B-Rep: UV-Net learns directly from parametric surfaces and curves,<sup>19</sup> while Hierarchical CADNet extracts machining features from B-Rep face-adjacency graphs using hierarchical message passing trained on the MFCAD++ corpus.<sup>20</sup> Hierarchical CADNet’s graph formulation directly inspired the Phase 5 GraphSAGE embedder. These geometric methods rest on foundational machine-learning advances. Graph Convolutional Networks (GCNs) introduced spectral graph convolutions for semi-supervised node classification,<sup>21</sup> and GraphSAGE generalized this to inductive learning on unseen nodes via neighbor sampling and aggregation,<sup>22</sup> making it directly applicable to STEP files the system has never encountered. PyTorch Geometric provides the implementation substrate widely used for these methods.<sup>23</sup> For visual verification, the Vision Transformer demonstrated that pure-attention architectures can match or exceed convolutional networks at image recognition,<sup>24</sup> underwriting the multimodal capability exploited in the GPT-4o verifier.<sup>25</sup>

These threads converge on a clear gap. Existing approaches address isolated sub-problems but stop short of closed-loop DFM repair: Text-to-CAD systems generate geometry from natural language yet cannot reason over or modify an existing part;<sup>7,26</sup> B-Rep feature-recognition networks classify face types with high accuracy but produce no geometric modifications in response;<sup>27</sup> and automated manufacturability-analysis tools predict non-manufacturable regions without generating corrective fixes.<sup>28,29</sup> None of these lines closes the loop where an existing CAD part is parsed, reasoned about, and modified back into a manufacturable form. This presents a question: Can an agentic LLM system automate Design for Manufacturing

for FDM? The focus would be on the tractable subset of automatically detecting overhangs and applying targeted DFM strategies to resolve them.

This work introduces *AgentsCAD* which takes in a STEP file with a manufacturing defect (e.g. overhang) and produces (1) a modified STEP file with overhangs resolved and (2) a human-readable report describing what was changed and why. The system is primarily composed of four core features. First, a JSON serialization of geometry-to-language representation is used to translate B-Rep geometry, topology, and shape descriptors into a compact LLM-readable prompt. Second, a blackboard multi-agent architecture <sup>30</sup> in which a shared-state orchestration pattern makes every phase interchangeable without modifying any other agent. Third, a hierarchical GraphSAGE feature embedder, a GNN trained on MFCAD++ dataset <sup>20</sup> that produces 25-class semantic face labels for injection into the LLM prompt, with a systematic comparison against a GCN baseline. Fourth, an end-to-end working demonstration of validated test parts of varying complexity, incorporating VLM-based visual verification and human-in-the-loop prompt engineering.

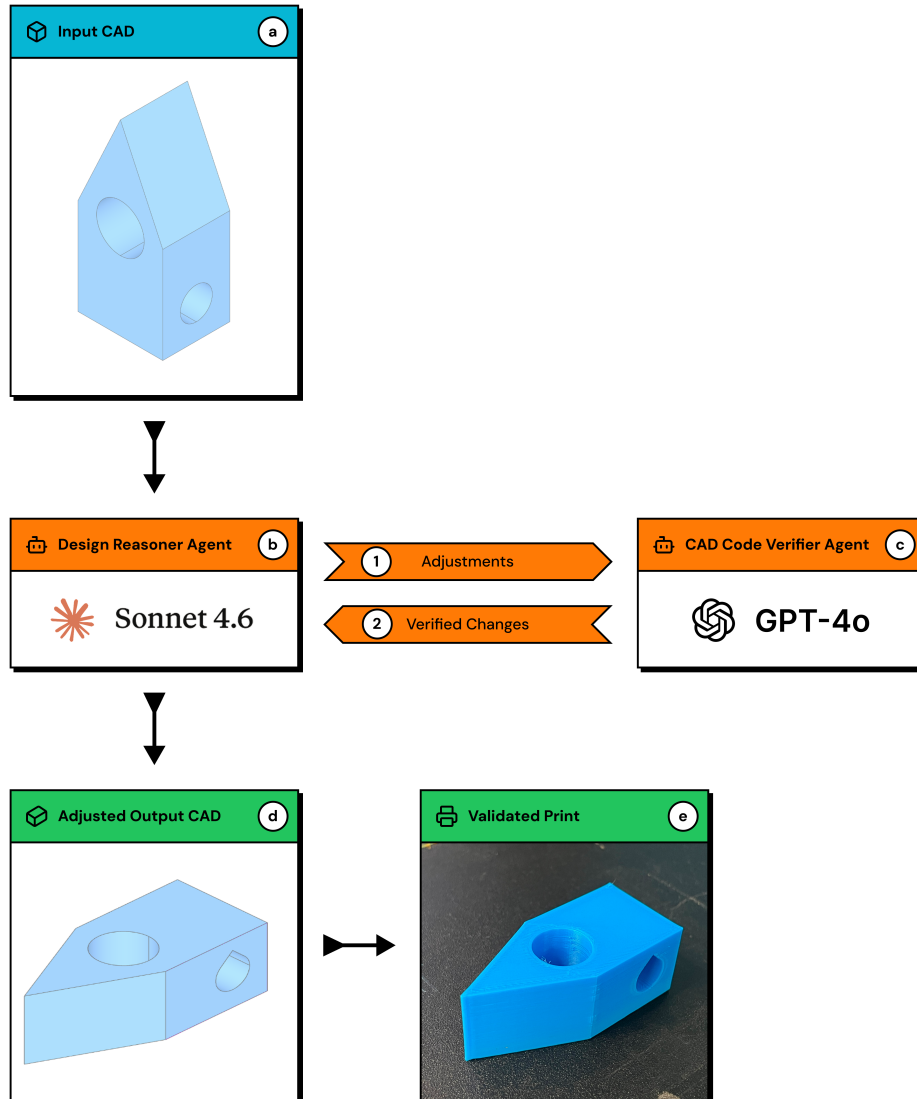


Figure 1: Agentic system for adapting CAD models for FDM 3D printing. Example (a) displays simplified bird house model with potential orientation and geometry adjustments. CAD model is delivered to the (b) Design Reasoner agent which provides suggestions and optimizations for adjustments which the (c) CAD Code Verifier Agent then evaluates. Iteration between the two agents proceed until a sufficient adjusted (d) output CAD model is generated and (e) validated via FDM 3D printing.

## 2 Related Works

LLM-3D Print by Jadhav et al.<sup>3</sup> explores the use of an agentic system for the purpose of FDM print optimization. In this work in-situ monitoring techniques via optical camera are

used to assess the quality of a print after each layer to detect potential FDM defects.<sup>3,31</sup> Unlike other related in-situ based monitoring techniques which utilize specialized models to detect specific features,<sup>32-38</sup> LLM3D print utilizes the base ChatGPT 4o to analyze the obtained images.<sup>3</sup> Utilizing custom firmware, the system is capable of executing real-time parameter changes through tool calling to repair builds optimizing on quality and defect reduction in the following layers.<sup>3</sup> The results of the agentic system were evaluated by a cohort of qualified engineers and mechanically validated with compression testing.<sup>3</sup> Additionally LLM3D print was evaluated on various multiple FDM printer setups, showcasing the agentic system's versatility on any commercial printer platform.<sup>3</sup>

In Agentic Additive Manufacturing Alloy Evaluation by Pak et al.,<sup>39</sup> the authors develop an agentic system for the search and evaluation of alloys suitable for fabrication via additive manufacturing. The developed system leverages the Model Context Protocol (MCP)<sup>40</sup> allowing for universal compatibility of the developed tools to various large language models. The system is composed of 3 main subagents including the workspace agent primarily involved with managing the output and folders of the two other agents those being the ThermoCalc subagent and the Additive Manufacturing subagent.<sup>39</sup> The ThermoCalc subagent utilizes TC Python in order to generate the material parameters such as solidus and liquidus temperatures and specific heat capacity values from an arbitrary elemental composition.<sup>39</sup> The Additive Manufacturing subagent is responsible for generating the process map of the given material parameters and a range of power and velocity combinations using Rosenthal's approximation of a melt pool.<sup>39,41</sup> From this work, it was shown that an agentic system is capable of generating preliminary lack of fusion process maps for various alloy compositions utilized for specific applications.<sup>39</sup>

RocketSmith<sup>42</sup> investigates the use of an agentic system to aid in the design and manufacturing of high powered rockets. This system combines the use of various tools including OpenRocket, CADSmith,<sup>9</sup> and PrusaSlicer to optimize over flight parameters such as stability, generate the associated parametric STEP files, and output the manufacturing designs and

files respectively. The system provides a graphical user interface allowing human-in-the-loop guidance and adjustment to design along with a collection of subagents and skills to aid with workflow specific tasks.<sup>42</sup> Four different rockets were generated using the agentic system and flight tested achieving a maximum altitude accuracy of 84% to the calculations.<sup>42</sup> Two of the four rockets were successfully recovered in re-flyable condition showcasing the agentic system’s capability to generate suitable designs for high powered rockets.

### 3 Background

#### 3.1 GCN

A Boundary Representation (B-Rep) solid encodes geometry as a graph whose nodes are faces and whose edges connect topologically adjacent faces. This native graph structure makes Graph Neural Networks (GNNs) the natural embedding tool. The Graph Convolutional Network (GCN) of Kipf and Welling<sup>21</sup> computes node representations by spectral convolution with a first-order localised filter. At each layer  $l$  the update rule is

$$\mathbf{H}^{(l+1)} = \sigma\left(\tilde{\mathbf{D}}^{-1/2}\tilde{\mathbf{A}}\tilde{\mathbf{D}}^{-1/2}\mathbf{H}^{(l)}\mathbf{W}^{(l)}\right), \tag{1}$$

where  $\tilde{\mathbf{A}} = \mathbf{A} + \mathbf{I}$  is the adjacency matrix with self-loops,  $\tilde{\mathbf{D}}$  is its degree matrix, and  $\sigma$  is a nonlinear activation.

#### 3.2 GraphSage

GraphSAGE<sup>22</sup> replaces GCNConv layers with SAGEConv at both levels of the B-AAG, while preserving the same two-level pooling structure, number of layers, hidden dimension, dropout, and classification head. GraphSAGE aggregates neighbor features separately and

*concatenates* the result with the node’s own current representation:

$$h_v^{(l+1)} = \sigma(W^{(l)} \cdot \text{CONCAT}(h_v^{(l)}, \text{MEAN}_{u \in \mathcal{N}(v)} h_u^{(l)})). \quad (2)$$

### 3.3 RAG

Large language models (LLMs) used in agentic systems lack persistent memory across invocations: each call begins with an empty context window, discarding any nuance accumulated over prior parts. Retrieval-Augmented Generation (RAG)<sup>43</sup> addresses this by conditioning generation on documents retrieved from an external index at inference time. In the original formulation, a dense retriever maps queries and documents into a shared vector space; at generation time, the  $k$  nearest documents are prepended to the prompt, grounding the model’s output in non-parametric, updatable knowledge.

## 4 Methods

### 4.1 Representational Challenges

Representing CAD geometry to an LLM is a non-trivial task.<sup>9,35,44</sup> A STEP file encodes thousands of faces, edges, and vertices in a binary B-Rep format that language models cannot parse directly. The initial hypothesis proposed that raw geometric scalars alone (surface normals, areas, centroids) would provide sufficient context for an LLM to reason about manufacturability. In practice this approach produced a representation that was simultaneously too verbose and too unstructured: the model received large arrays of floating-point numbers with no indication of what those values mean in a manufacturing context, and spatial relationships between adjacent faces were entirely absent. A face with a downward normal adjacent to a cylindrical surface is almost certainly a through-hole, but without a semantic label the model must infer this solely from numerical primitives. Equally, no single fix resolves every overhang. The same downward-facing face may call for a fillet, a

reorientation, or a part split depending on surrounding context.

CadQuery provided a Python interface to traverse the B-Rep topology of a loaded STEP file, exposing each face as a structured object with a semantic surface-type label: Planar, Cylinder, Cone, or BSpline alongside area, outward normal, and centroid. After parsing, every face is described by features such as its surface type, area, centroid, and signed tilt angles. The `radius_of_gyration_mm` indicates the approximate footprint on the build surface, while the `elongation_index` captures how lopsided that footprint is, allowing faces of similar area but different shape to be distinguished. At the part level, a total bounding box and centre of mass anchor the spatial reasoning. Where higher-fidelity analysis was required, the underlying OpenCASCADE (OCCT) kernel was called directly: surface-property routines extract the inertia tensor per face, from which radius of gyration and elongation index are derived as stability proxies; parametric UV-space sampling via BRepAdaptor surfaces captures curvature variation across each face. Equally important, OCCT’s edge-to-face topology traversal maps shared-edge adjacency between faces, encoding the spatial relationships that a flat scalar array cannot represent. Together these two layers produce a structured intermediate representation. Semantic type labels, orientation metrics, and an explicit face adjacency graph. This is legible to a language model where the raw binary STEP format is not, and that carries enough topological context to support inferences of the kind illustrated above: a planar face sharing an edge with a cylindrical face is a candidate through-hole; absent that adjacency, the model has only a normal vector and an area to reason from. Any usable representation must therefore *preserve enough spatial and topological context to make a contextual decision possible* while remaining compact enough to fit inside a model’s context window. The complete prompt is a single JSON object containing `features`, `links`, and `overhangs` sections. This representation provides a sufficient amount of context for the LLM to reason over individual faces by ID while remaining compact enough to leave headroom for CoT output and tool-use turns. Lastly, With GraphSAGE weights present, each face is augmented using a `feature_type` label (e.g. `rect_pocket`, `chamfer`) and a `feature_confidence` score, and these fields are

folded into both the per-face record and the adjacency descriptions. The topology graph is serialized into a `links` list of `adjacent_to` relations between face IDs.

## 4.2 System Architecture

### 4.2.1 Blackboard Architecture for Multi-Agent Coordination

Multi-agent LLM frameworks such as LangChain and CrewAI impose a conversational or role-based execution model in which agents communicate via message passing, making it difficult to enforce strict phase ordering, inject deterministic rule-based stages, or swap individual models without refactoring the coordination logic. AgentsCAD instead organises its pipeline around the *blackboard pattern*,<sup>30</sup> a classical architecture in which a single shared-state object is read and written by independent agents in a fixed phase order. This design decouples every phase from every other: modifying the geometry parser requires changing only that agent and one configuration entry, leaving the downstream reasoner and verifier untouched. Three further properties motivated this choice. *Deterministic floor*: initial defect identification is entirely rule-based, flagging any face whose surface normal satisfies  $\theta = \arccos(\hat{n}_{\text{face}} \cdot \hat{z}_{\text{plane}}) \leq 0$  as a potential overhang without invoking an LLM. This establishes a verifiable ground truth that the language model never has to reproduce and cannot corrupt. *State-reactivity*: agents read the blackboard between phases and conditionally trigger or skip downstream work based on prior output; if the reasoner finds no printability concerns, the modifier and verifier phases are skipped entirely, avoiding unnecessary API calls. *Dual-model deployment*: the reasoning phase is handled by Claude Sonnet 4.6 using chain-of-thought prompting,<sup>45</sup> while a separate GPT-4o instance serves as the vision-language verifier; the blackboard pattern makes it trivial to replace either model independently, as neither agent has knowledge of the other’s identity.

### 4.2.2 Agentic System

The system is carried out through nine phases with two conditional sub-phases (Figure 1).

The system first imports the `STEP` file and extracts several scalar attributes per face which

include: surface type, area, centroid coordinates, axis signed tilt angles, radius of gyration, and a unitless elongation index distinguishing dense from needle-like geometry. Bounding box and center of mass are written to a shared blackboard for downstream access. From there, every face normal is compared against the build plane’s z-axis using the arccosine of their dot product, and any face at or below zero degrees is flagged as an overhang. The part is then rendered as either a static PNG or an interactive 3D environment for human inspection, establishing the visual baseline the verifier will use later. Shared-edge adjacencies are resolved next and written to the blackboard as a JSON adjacency structure. A GraphSAGE model pretrained on 59,665 parts then produces 128-dimensional embeddings and 25-class semantic feature predictions per face; when pretrained weights are unavailable, node2vec embeddings are substituted, which are retained locally but withheld from the language model so the system can continue on geometry and topology alone. With the blackboard fully populated, the assembled JSON prompt is passed to the design reasoning module, which applies chain-of-thought (CoT)<sup>46</sup> reasoning grounded by MCP tools to recommend geometric changes. A scripted orientation sub-phase evaluates up to four candidate rotations and commits to the best one before any modification is made. The recommended operations (fillets, chamfers, teardrops, extrusions) are then applied programmatically, and the resulting geometry is rendered and inspected by a vision-language model to verify the changes visually. The system workflow concludes by writing the optimized STEP file, a verification render, a plain-text recommendations file, and a full blackboard snapshot for human review.

## **4.3 Evolving Geometric Understanding: GCN to GraphSAGE to RAG**

### **4.3.1 Motivation**

Raw scalar geometry exposed a fundamental tension. The LLM received large arrays of numbers (normals, areas, tilt angles) but it had no indication of what those primitives meant

in a manufacturing context nor did it capture inter-face geometric relationships in the scalar representation. Pockets, slots, and steps are defined by *how faces relate to one another*, not by any single face in isolation. This motivated injecting learned semantic feature labels via a graph neural network trained on MFCAD++.

### 4.3.2 Baseline: Hierarchical GCN

<sup>21</sup> GCN is applied hierarchically across the two-level Bipartite Attributed Adjacency Graph (B-AAG) structure of MFCAD++, stacking three GCNConv layers (hidden dim 64, dropout 0.5) at each level. GCN is an appropriate baseline because the B-Rep face-adjacency graph is the native data format and *homophily* holds strongly: faces belonging to the same machining feature are topologically adjacent by construction. However, GCN is *transductive*, it learns node embeddings tied to a fixed training graph and cannot generalize to unseen graphs without retraining. In MFCAD++, each of the 59,665 parts is a separate graph of different sizes and topology, which makes transductive inference incompatible with the deployment scenario. Additionally, GCN’s symmetric normalization dilutes each face’s own geometric attributes into the neighborhood aggregate, damaging recognition of minority classes whose distinctive local geometry is the primary distinguishing signal.

### 4.3.3 Variant: Hierarchical GraphSAGE

The concatenation structure of GraphSAGE has two consequences that are critical for CAD-geometry inference. First, *inductiveness*: because GraphSAGE learns an aggregation function rather than per-node embeddings, the trained model can produce embeddings for faces on entirely new parts at test time. This is essential for AgentsCAD, where the model is expected to classify faces on user-supplied STEP files it has never encountered. Second, *self-feature preservation*: each face’s own geometric attributes (surface type, area, centroid, tilt angles, radius of gyration) are carried forward as a direct input to every layer, ensuring they are never overwritten by neighbourhood averaging. This is particularly valuable for rare feature types

such as *triangular through slot* or *slanted through step*, whose primary distinguishing signal is their local geometry rather than their graph neighbourhood. AgentsCAD applies GraphSAGE hierarchically across the two-level Bipartite Attributed Adjacency Graph (B-AAG) structure of MFCAD++, stacking three SAGEConv layers (hidden dimension 64, dropout 0.5) at each level. Face-level input features are optionally augmented with UV-sampled surface normals following UV-Net,<sup>19</sup> adding mean normal, normal standard deviation, and a UV-coverage ratio to the base five-dimensional per-face descriptor.

#### 4.3.4 Feature augmentation: UV-net surface normals

Beyond the architectural variant, this work evaluates augmenting the face-level node features  $V_1$  with UV-sampled surface normals from the underlying B-Rep geometry, following UV-Net.<sup>19</sup> For each face a  $5 \times 5$  UV grid (retaining only points that pass the trim-boundary test) is sampled followed by the computation of three additional descriptors: mean surface normal (3D), normal standard deviation (3D), and UV coverage ratio (1D). These 7 descriptors are concatenated with the existing 5-dimensional  $V_1$  features, producing a 12-dimensional face input. This augmentation applies to both GCN and GraphSAGE, allowing independent evaluation of the architectural and feature-level contributions independently.

#### 4.3.5 RAG memory

Even with learned semantic labels, the reasoning agent lacks memory across parts. In AgentsCAD, RAG serves as a *cross-part memory layer*. After each analysis, the blackboard state (geometry descriptors, feature predictions, and the LLM’s reasoning trace) is encoded as a 256-dimensional context vector and indexed in a FAISS store. When analysing a new part, the  $k$  most similar past decisions are retrieved and prepended to the reasoning prompt. This allows the system to accumulate technical nuance over time without retraining the underlying GNN or fine-tuning the LLM. For example, learning that teardrop modifications are unreliable on holes wider than 50 mm, or that certain feature combinations reliably call for a split

rather than a fillet. This enables the system to improve steadily as it processes more parts, without retraining the underlying model. The RAG layer therefore converts agentsCAD from a stateless classifier into a system that improves monotonically as it processes more parts.

## 4.4 Design Reasoning Agent

The Design Reasoner is a Claude Sonnet 4.6 agent provided with the assembled JSON geometry prompt and a comprehensive manufacturing system prompt encoding DFM heuristics: angle conventions, overhang severity thresholds, stability criteria, and modification trade-offs. The agent uses CoT reasoning to analyze the model for overhangs, print stability, stress concentrations, and thin features, following a mandatory decision order. First, reorientation is considered globally: the agent calls `check_orientation_overhangs` to ground the proposed rotation in computed geometry, then calls `lay_face_to_build_surface` to compute exact  $x/y$  rotation angles for a target face. Second, local modifications, such as fillet, chamfer, and teardrop, are applied after the orientation is fixed. Third, support structures are flagged when no geometric fix suffices. Fourth, splitting the part is used as a last resort and overrides all other actions when invoked.

The two MCP tools ground the agent’s “mental rotation” in real geometry, preventing the coordinate-transform hallucinations that arise when an LLM must reason about 3-D rotations from text alone. The agent returns a typed JSON recommendations dictionary consumed directly by Phase 7.

## 4.5 Part Modification

The JSON modification recommendations are assigned by target `face_id` and programmatically executed via CadQuery. The reorient operation is always performed *last*, because reinterpreting the STEP file after rotation reallocates `face_id` values, which would invalidate any earlier face-specific operations.

## 4.6 Visual Verification

The verifier is a novel adaptation of CADCodeVerify,<sup>11</sup> originally proposed for validating generated CAD code, repurposed here for geometry modification. After the modifier applies a set of operations, the part is rendered from four angles into a  $2 \times 2$  composite at  $2048 \times 2048$  pixels with edges visible. The system then generates one targeted yes/no question per applied modification (e.g. for a fillet, “Do edges of *face\_X* appear smoothly rounded ( $\sim R$  mm)?”) together with general integrity and overhang questions that always run, catching silent modifier failures even when no operation was applied. GPT-4o replies Yes/No/Unclear with a chain-of-thought rationale; failures are logged to the blackboard.

## 4.7 Human-in-the-Loop Validation

Beyond automated VLM verification, the development of a solidified workflow relied heavily on a *prompt-to-structure* approach in which the authors’ manufacturing expertise was used to design the system prompt and MCP tool schemas that scaffold the LLM’s reasoning toward correct DFM logic. This process was iterative: each test case exposed gaps in the agent’s reasoning that were closed by tightening angle conventions, adding mandatory tool-call sequences, or expanding the modification action space. Structured prompt engineering proved as important as any architectural choice: an LLM without geometric grounding consistently hallucinated rotations, while the same model with the `check_orientation_overhangs` tool and explicit angle invariants produced reliable, physically valid plans.

# 5 Results and Discussion

## 5.1 Graph Embedder: GCN vs. GraphSAGE

Table 1 reports test-set performance across all model configurations on the MFCAD++ held-out split. Macro F1 is the primary metric: it computes F1 independently for each of

the 25 classes and averages without weighting by class frequency, appropriately penalizing failures on rare feature types.

Table 1: Test-set performance across all model configurations on MFCAD++. Macro F1 is the primary metric. Best result per column in **bold**.

Architecture	Features	Accuracy	Macro F1	Macro Prec.	Macro Rec.
GCN (baseline)	$V_1$ only	0.443	0.338	0.336	0.396
GCN	$V_1+V_2$	0.363	0.306	0.345	0.377
GCN	UV-net	0.538	0.469	0.472	0.552
GraphSAGE	$V_1$ only	0.638	0.545	0.534	0.579
GraphSAGE	$V_1+V_2$	0.794	0.727	0.716	0.753
GraphSAGE	UV-net	<b>0.850</b>	<b>0.785</b>	<b>0.774</b>	<b>0.805</b>

### 5.1.1 GraphSAGE vs. GCN

GraphSAGE outperforms GCN across all three feature representations, confirming the primary hypothesis. On  $V_1$ -only features, GraphSAGE achieves a macro F1 of 0.545 versus GCN’s 0.338, a 61% relative improvement from the architectural change alone. With UV-net augmentation, GraphSAGE reaches 0.785 F1 and 85.0% accuracy versus GCN’s 0.469 F1 and 53.8% accuracy. The performance gap widens as feature richness increases, suggesting that GraphSAGE’s concatenation-based aggregation is better equipped to exploit additional information than GCN’s normalized averaging.

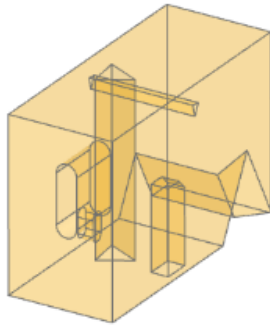
### 5.1.2 Effect of hierarchical aggregation

The  $V_1 \rightarrow V_1+V_2$  transition has starkly different effects on the two architectures. For GraphSAGE, adding the facet-level pass yields the largest single improvement of any step: F1 increases from 0.545 to 0.727 (+0.182). For GCN, the same addition *decreases* performance: F1 drops from 0.338 to 0.306. This counterintuitive result is consistent with GCN’s symmetric normalization, which merges pooled facet context into the face representation via a weighted sum, diluting the face’s own geometry. GraphSAGE’s explicit concatenation preserves self-features, allowing the richer hierarchical signal to help rather than hurt.

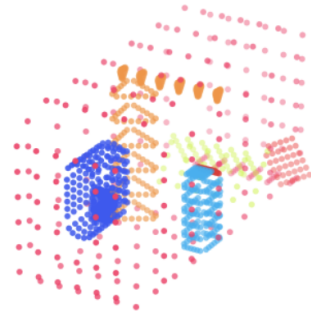
### 5.1.3 MeshViz: Prediction visualization on B-Rep Geometry

MeshViz, is a post-training visualization tool that renders model predictions directly onto B-Rep face geometry. It is used to ground the quantitative results in geometric intuition. After training concludes, MeshViz loads the STEP file for each sampled test part via CadQuery, runs inference on the corresponding held-out test graph, and tessellates each face’s 3D surface by sampling an  $8 \times 8$  UV grid over the parametric domain via the OpenCASCADE kernel, discarding points that fall outside the face’s trim boundary. Each face’s resulting point cloud is colored by prediction outcome: the face’s assigned class color if the prediction matches the ground-truth label, and red otherwise. The colored point clouds are logged to W&B as interactive Object3D objects for real-time inspection during experiment tracking, then rendered as static figures for this paper. Figure 2 shows representative samples from the best model (GraphSAGE UV-net).

The visualizations reveal that misclassified faces cluster at feature boundaries (the transition zones between a machining feature and the surrounding stock material). Interior faces of well-defined features are almost universally correctly classified, while boundary faces are consistently confused with adjacent feature types or the base stock. This is geometrically interpretable: boundary faces have mixed neighborhoods containing both feature-internal and feature-external adjacency, producing ambiguous aggregated representations regardless of the aggregation operator used. This finding suggests that boundary-aware loss weighting or explicit boundary detection as an auxiliary task could be a productive direction for future work.



(a) Original Part



(b) Predicted (97% face acc.)

Figure 2: Per-face feature classification visualization for a simple part (GraphSAGE+UV-net). Predicted faces are colored by class; red faces are misclassified.

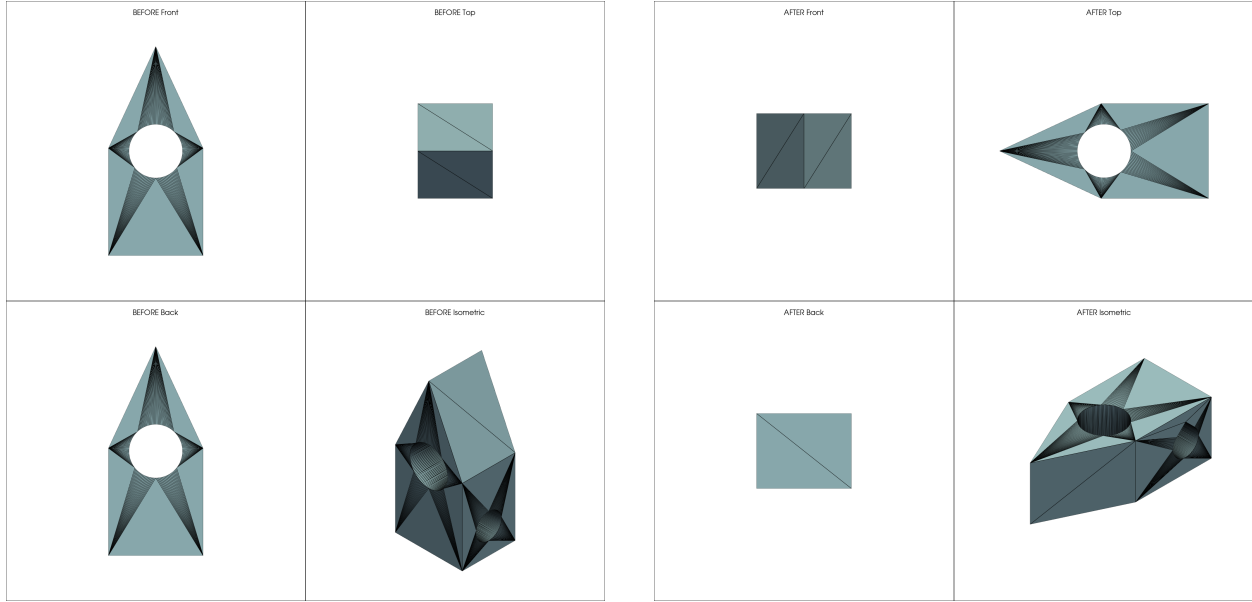
## 5.2 Test Case Validation

The end-to-end functionality was validated on two test parts of differing complexity. The tests were aimed to make sure the system could make consistent modification operations, provide consistent independent reasoning as well verify print stability. All renderings show the original part and orientation as well as the finished product following the system implementation.

### 5.2.1 Birdhouse

The birdhouse is a nine-face solid combining seven planar faces with two cylindrical bores (`face_4` and `face_8`). In the default Z-up orientation both bores presented as severe overhangs (tilt  $-90^\circ$ ), flagged as actionable by the rule-based overhang detector. Prior to LLM reasoning, the RAG pipeline retrieved domain knowledge on horizontal bores and teardrop compensation, injecting it directly into the prompt and priming the reasoner with established FDM heuristics before any tool calls were made. The design reasoner issued six tool calls to evaluate candidate orientations, calling `check_orientation_overhangs` to probe  $90^\circ$  rotations about each axis

and `lay_face_to_build_surface` to obtain exact Euler angles for three candidate bed faces before settling on a recommendation. The StrategyCouncil overrode the LLM’s reorient target in favour of the bore-side-lay heuristic: laying `face_6` (1,463 mm<sup>2</sup>) flat on the bed at  $X = 90^\circ$  aligned the bore axis of `face_4` with the build direction, eliminating it entirely. One bore (`face_8`) remained horizontal after reorientation. The council correctly rejected two spurious chamfer candidates, one on the print-bed face and one on a vertical wall, before unanimously selecting a teardrop modification for the remaining bore. The modifier applied the teardrop to `face_8`, expanding the face count from 9 to 12, and a post-modification overhang recheck confirmed zero actionable overhangs on the final geometry. OCCT solid validation passed with a volume delta of  $-0.75\%$ , consistent with the small material removal expected from a teardrop profile. The VLM verifier returned two inconclusive flags on wall thickness and cross-sectional area; both were attributable to insufficient render resolution rather than genuine geometry defects, as the verifier’s own reasoning acknowledged the modifications were consistent with the intended teardrop action and that the renders did not provide sufficient detail for a definitive assessment. The complete resolution sequence, two initial overhangs, one eliminated by reorientation, one resolved by teardrop modification, was achieved in a single pipeline iteration.



(a) Original Birdhouse CAD input

(b) Modified Birdhouse CAD output

### 5.3 Ablation: MCP Grounding Tools

A key design question was whether tool-use grounding is necessary or whether the LLM can reason about 3-D rotations from the JSON representation alone. In early runs without the `check_orientation_overhangs` and `lay_face_to_build_surface` MCP tools, the agent consistently hallucinated rotation angles, proposing, for example, a  $+45^\circ$  rotation for a face whose correct reorientation requires  $-30^\circ$ , then asserting with high confidence that the result was overhang-free. With both tools enabled, coordinate-transform errors were eliminated across all test cases: the agent first queries the tool for the required rotation, then verifies the post-rotation overhang map before committing. This ablation confirms that geometric grounding via MCP tools is *not* an optional enhancement but a prerequisite for reliable DFM reasoning.

## 6 Conclusion

AgentsCAD demonstrates that raw STEP files can be turned into DFM-improved parts by an agentic, blackboard-orchestrated system combining a deterministic geometry parser, a Claude Sonnet design-reasoner with a small library of grounding tools, and a GPT-4o visual verifier. The system bridges the gap between B-Rep geometry and LLM reasoning for the targeted problem of overhang resolution, producing physically valid modified STEP files and emitting human-readable manufacturing reports.

Three findings stand out. First, structured JSON geometry with explicit topology instead of raw scalar arrays proves to be sufficient for an LLM to perform contextual DFM reasoning, including stability analysis that goes beyond overhang detection. Second, GraphSAGE’s inductive, self-feature-preserving aggregation outperforms GCN across all feature sets, with the largest gains on richer representations where GCN’s normalized averaging actively hurts minority-class recognition. Third, MCP tool grounding is not an enhancement but a prerequisite: without it, the agent hallucinates coordinate transforms with high confidence.

## 7 Future Work

Larger parts incur both context-size pressure and “lost-in-the-middle” effects as face counts grow, and the current prompt does not decimate or summarize sub-graphs. The system uses a single agent for all DFM facets; decomposing reasoning into dedicated sub-agents (e.g. a stress-concentration specialist) would improve coverage. The system currently accepts only single parts with no assembly support.

Four immediate extensions emerge from this work: a **SplitAgent** that partitions parts at LLM-specified planes; active GraphSAGE injection replacing prompt-based geometric primitives with topology embeddings consumed directly by the reasoner; expansion of the RAG memory to accumulate technical nuance across a growing library of parts; and defect-class expansion to robustly detect bridges, thin features, and internal bores. On a longer

horizon, GPT-5's demonstrated capability for generating native CAD representations and interpreting open-ended user modification requests positions it as a natural upgrade for the Design Reasoner, possibly enabling the system to move beyond structured JSON prompts toward conversational, multimodal DFM collaboration with the full expressiveness of natural language.

## References

- (1) Rajan, K.; Samykano, M.; Kadirgama, K.; Harun, W. S. W.; Rahman, M. M. Fused deposition modeling: process, materials, parameters, properties, and applications. *The International Journal of Advanced Manufacturing Technology* **2022**, *120*, 1531–1570.
- (2) Pak, P.; Farimani, A. B. AdditiveLLM2: A Multi-modal Large Language Model for Additive Manufacturing. 2026; <http://arxiv.org/abs/2603.22017>, arXiv:2603.22017 [cs.LG].
- (3) Jadhav, Y.; Pak, P.; Barati Farimani, A. LLM-3D print: Large Language Models to monitor and control 3D printing. *Additive Manufacturing* **2025**, *114*, 105027.
- (4) Thompson, M. K.; Moroni, G.; Vaneker, T.; others Design for Additive Manufacturing: Trends, Opportunities, Considerations, and Constraints. *CIRP Annals* **2016**, *65*, 737–760.
- (5) Zhang, L.; Le, B.; Akhtar, N.; Lam, S.-K.; Ngo, T. Large Language Models for Computer-Aided Design: A Survey. *ACM Computing Surveys* **2026**, *58*, Article 225.
- (6) Zhang, L.; Le, B.; Akhtar, N.; Lam, S.-K.; Ngo, T. LLMs for CAD: A Survey on Large Language Models for Computer-Aided Design. *ACM Computing Surveys* **2025**, *37*, Article 111.
- (7) Khan, M. S.; Sinha, S.; Sheikh, T. U.; Stricker, D.; Ali, S. A.; Afzal, M. Z. Text2CAD: Generating Sequential CAD Models from Beginner-to-Expert Level Text Prompts. *arXiv preprint arXiv:2409.17144* **2024**,
- (8) Badagabettu, A.; Yarlagadda, S. S.; Farimani, A. B. Query2CAD: Generating CAD Models Using Natural Language Queries. *arXiv preprint* **2024**,
- (9) Barkley, J.; Loghmani, R.; Farimani, A. B. CADSmith: Multi-Agent CAD Genera-

- tion with Programmatic Geometric Validation. 2026; <https://arxiv.org/abs/2603.26512v1>.
- (10) Tang, J.; Xiao, H.; Li, X.; Wang, W.; Gong, Z. ChatCAD: An MLLM-Guided Framework for Zero-Shot CAD Drawing Restoration. IEEE International Conference on Multimedia and Expo. 2026.
  - (11) Alrashedy, K.; Tambwekar, P.; Zaidi, Z.; Langwasser, M.; Xu, W.; Gombolay, M. Generating CAD Code with Vision-Language Models for 3D Designs. International Conference on Learning Representations. 2025.
  - (12) Pak, P.; Farimani, A. B. AdditiveLLM: Large Language Models Predict Defects in Metals Additive Manufacturing. *arXiv preprint* **2025**,
  - (13) Petsiuk, A.; Pearce, J. M. Real-Time Defect Detection for FFF 3D Printing Using Lightweight Model Deployment. *arXiv preprint* **2023**,
  - (14) Shah, J. J.; Anderson, D.; Kim, Y. S.; Joshi, S. A Discourse on Geometric Feature Recognition From CAD Models. *Journal of Computing and Information Science in Engineering* **2000**, *1*, 41–51.
  - (15) Babić, B. R.; Nešić, N.; Miljković, Z. Automatic Feature Recognition Using Artificial Neural Networks to Integrate Design and Manufacturing: Review of Automatic Feature Recognition Systems. *Artificial Intelligence for Engineering Design, Analysis and Manufacturing* **2011**, *25*, 289–304.
  - (16) Onwubolu, G. C. Manufacturing Features Recognition Using Backpropagation Neural Networks. *Journal of Intelligent Manufacturing* **1999**, *10*, 289–299.
  - (17) Wu, Z.; Song, S.; Khosla, A.; Yu, F.; Zhang, L.; Tang, X.; Xiao, J. 3D ShapeNets: A Deep Representation for Volumetric Shapes. IEEE Conference on Computer Vision and Pattern Recognition. 2015; pp 1912–1920.

- (18) Lee, J.; Lee, H.; Mun, D. 3D Convolutional Neural Network for Machining Feature Recognition with Gradient-Based Visual Explanations from 3D CAD Models. *Scientific Reports* **2022**, *12*, 14864.
- (19) Jayaraman, P. K.; Sanghi, A.; Lambourne, J. G.; Willis, K. D. D.; Davies, T.; Shayani, H.; Morris, N. UV-Net: Learning from Boundary Representations. *arXiv preprint arXiv:2006.10211* **2021**,
- (20) Colligan, A. R.; Robinson, T. T.; Nolan, D. C.; Hua, Y.; Cao, W. Hierarchical CADNet: Learning from B-Reps for Machining Feature Recognition. *Computer-Aided Design* **2022**, *147*, 103226.
- (21) Kipf, T. N.; Welling, M. Semi-Supervised Classification with Graph Convolutional Networks. International Conference on Learning Representations. 2017.
- (22) Hamilton, W. L.; Ying, R.; Leskovec, J. Inductive Representation Learning on Large Graphs. Advances in Neural Information Processing Systems. 2017.
- (23) Fey, M.; Lenssen, J. E. Fast Graph Representation Learning with PyTorch Geometric. ICLR Workshop on Representation Learning on Graphs and Manifolds. 2019.
- (24) Dosovitskiy, A.; Beyer, L.; Kolesnikov, A.; Weissenborn, D.; Zhai, X.; Unterthiner, T.; Dehghani, M.; Minderer, M.; Heigold, G.; Gelly, S.; Uszkoreit, J.; Houlsby, N. An Image is Worth 16x16 Words: Transformers for Image Recognition at Scale. International Conference on Learning Representations. 2021.
- (25) OpenAI *GPT-4o System Card*; 2024; arXiv:2410.21276.
- (26) Wu, R.; Xiao, C.; Zheng, C. DeepCAD: A Deep Generative Network for Computer-Aided Design Models. Proceedings of the IEEE/CVF International Conference on Computer Vision (ICCV). 2021; pp 6772–6782.

- (27) Wu, H.; Lei, R.; Peng, Y.; Gao, L. AAGNet: A Graph Neural Network towards Multi-task Machining Feature Recognition. *Robotics and Computer-Integrated Manufacturing* **2024**, *86*, 102661.
- (28) Balu, A.; Ghadai, S.; Young, G.; Sarkar, S.; Krishnamurthy, A. A Machine-Learning Framework for Design for Manufacturability. *arXiv preprint arXiv:1703.01499* **2017**,
- (29) Zhong, F.; Wang, Y.; Wang, P.-S.; Lu, L.; Zhao, H. DeepMill: Neural Accessibility Learning for Subtractive Manufacturing. *ACM SIGGRAPH Conference Papers*. 2025.
- (30) Hayes-Roth, B. A Blackboard Architecture for Control. *Artificial Intelligence* **1985**, *26*, 251–321.
- (31) Hu, W.; Chen, C.; Su, S.; Zhang, J.; Zhu, A. Real-time defect detection for FFF 3D printing using lightweight model deployment. *The International Journal of Advanced Manufacturing Technology* **2024**, *134*, 4871–4885.
- (32) Pak, P.; Ogoke, F.; Polonsky, A.; Garland, A.; Bolintineanu, D. S.; Moser, D. R.; Arnhart, M.; Madison, J.; Ivanoff, T.; Mitchell, J. ThermoPore: Predicting part porosity based on thermal images using deep learning. *Additive Manufacturing* **2024**, *95*, 104503.
- (33) George, A.; Chen, Y.; Dikshit, A.; Gano, S.; Pak, P.; Farimani, A. B. BeadSight: An Inexpensive Tactile Sensor Using Hydrogel Beads. *IEEE Sensors Journal* **2024**, *25*, 35534–35540.
- (34) Bostan, B.; Hinnebusch, S.; Anderson, D.; To, A. C. Accurate detection of local porosity in laser powder bed fusion through deep learning of physics-based in-situ infrared camera signatures. *Additive Manufacturing* **2025**, *101*, 104701.
- (35) Wang, Z.; Jadhav, Y.; Pak, P.; Farimani, A. B. Image2Gcode: Image-to-G-code generation for additive manufacturing using diffusion-transformer model. *Additive Manufacturing Letters* **2026**, 100374.

- (36) Ogoke, F.; Pak, P.; Myers, A.; Quirarte, G.; Beuth, J.; Malen, J.; Farimani, A. B. Deep learning for melt pool depth contour prediction from surface thermal images via vision transformers. *Additive Manufacturing Letters* **2024**, *11*, 100243.
- (37) Ogoke, F.; Suresh, S. K.; Adamczyk, J.; Bolintineanu, D.; Garland, A.; Heiden, M.; Barati Farimani, A. Deep learning based optical image super-resolution via generative diffusion models for layerwise in-situ LPBF monitoring. *Additive Manufacturing* **2025**, *107*, 104790.
- (38) Ogoke, F.; Lee, W.; Kao, N.-Y.; Myers, A.; Beuth, J.; Malen, J.; Barati Farimani, A. Convolutional neural networks for melt depth prediction and visualization in laser powder bed fusion. *The International Journal of Advanced Manufacturing Technology* **2023**, *129*, 3047–3062.
- (39) Pak, P.; Chandrasekhar, A.; Farimani, A. B. Agentic additive manufacturing alloy evaluation. *Additive Manufacturing Letters* **2026**, 100355.
- (40) Anthropic Introducing the Model Context Protocol. <https://www.anthropic.com/news/model-context-protocol>.
- (41) Rosenthal, D. The Theory of Moving Sources of Heat and Its Application to Metal Treatments. *Transactions of the American Society of Mechanical Engineers* **2022**, *68*, 849–865.
- (42) Pak, P.; Barkley, J.; Loghmani, R.; Baich, D.; Pamal, A.; Farimani, A. B. RocketSmith: An Agentic System for High-Powered Rocket Design and Manufacturing. 2026; <http://arxiv.org/abs/2606.00097>, arXiv:2606.00097 [cs.RO].
- (43) Lewis, P.; Perez, E.; Piktus, A.; Petroni, F.; Karpukhin, V.; Goyal, N.; Küttler, H.; Lewis, M.; Yih, W.-t.; Rocktäschel, T.; Riedel, S.; Kiela, D. Retrieval-Augmented Generation for Knowledge-Intensive NLP Tasks. *Advances in Neural Information Processing Systems (NeurIPS)*. 2020; pp 9459–9474.

- (44) Jadhav, Y.; Barati Farimani, A. Large language model agent as a mechanical designer. *Journal of Engineering Design* **2026**, *0*, 1–37, \_eprint: <https://doi.org/10.1080/09544828.2026.2624356>.
- (45) Wei, J.; Wang, X.; Schuurmans, D.; Bosma, M.; Xia, F.; Chi, E.; Le, Q. V.; Zhou, D. Chain-of-Thought Prompting Elicits Reasoning in Large Language Models. *Advances in Neural Information Processing Systems (NeurIPS)*. 2022.
- (46) Wei, J.; Wang, X.; Schuurmans, D.; Bosma, M.; Ichter, B.; Xia, F.; Chi, E.; Le, Q.; Zhou, D. Chain-of-Thought Prompting Elicits Reasoning in Large Language Models. 2023; <http://arxiv.org/abs/2201.11903>, arXiv:2201.11903 [cs].